Enabling two-dimensional optical subdiffraction imaging at an extended working distance: a planar antenna-array approach

Yan Wang, Amr S. Helmy, and George V. Eleftheriades*

The Edward S. Rogers Sr. Department of Electrical and Computer Engineering, University of Toronto, 40 St. George Street, Toronto, Ontario M5S 2E4, Canada
**Corresponding author: gelefth@waves.utoronto.ca*

Received January 12, 2012; revised February 28, 2012; accepted February 28, 2012; posted February 29, 2012 (Doc. ID 161378); published April 30, 2012

We propose a practical optical probe configuration capable of two-dimensional subdiffraction imaging beyond the conventionally used near-field range. The probe consists of a planar array of plasmonic monopoles radiating with different amplitudes and phases, such that the near-field interaction of the array elements produces a subdiffraction spot size 40% smaller than the diffraction limit at a quarter-wavelength away from the probe. Although designed to operate in the visible, this topology is scalable to other spectra as well. Our proposed configuration could alleviate the "working distance" issue between the object and imaging apparatus since it enables superresolution focusing at relatively long distances while being compatible with existing near-field imaging setups, such as scanning near-field optical microscopes.

OCIS codes: 310.6628, 180.4243.

1. INTRODUCTION

One propitious route to achieving subdiffraction imaging is by ensuring sufficient contribution of evanescent waves at the image location in order to support the required resolution. Previous theoretical and experimental studies employing metamaterial superlenses have exploited the phenomenon of growing evanescent waves inside the lens, which enables the recovery of high-spatial components at the image location [1–3]. Although there is no theoretical limit on the working distance (distance between the object and imaging apparatus) for these techniques, practical constraints, in particular material losses, strongly hinder their performance. As a result, most of the experiments to date based on these techniques have demonstrated imaging distances of the order of $\lambda/10$.

A popular and more practical subdiffraction imaging technique, known as scanning near-field optical microscopy (SNOM/NSOM), collects evanescent fields directly through raster scanning of a sharp tip over the sample in its extreme near-field [4]. This technique requires the probe and the sample to be maintained extremely close (with a distance ranging from a few nanometers to a few tens of nanometers) at all times. Probing farther away severely diminishes the resolution quality due to diffraction. However, a longer "working distance" is desirable for numerous situations, including imaging sensitive specimens, such as biological samples, and objects buried inside dielectric media. Moreover, the near-field information can be observed more accurately owing to the reduced disturbance from the invasive presence of imaging probes in the extreme near-field. Furthermore, from the instrumentation point of view, probing at a longer distance could reduce the overall complexity of the SNOM system since one of the most complicated and costly components is the feedback system that precisely controls the probe-to-sample distance.

Recently, a technique based on the "near-field interference," also known as "radiationless interference," has been proposed as an alternative method for achieving superfocusing [5]. Similar to the Fresnel zone plates that focus propagating waves in the far field, the proposed near-field plates focus evanescent waves. However, unlike Fresnel zone plates, the focal spot size can be arbitrarily small due to the "static" nature of the evanescent wave interference. In the initial proposal, this technique was implemented using capacitive near-field plates, where the one-dimensional (1D) subwavelength focusing was demonstrated at microwave frequencies for working distances also of the order of $\lambda/10$ [6].

A related but alternative implementation of near-field superfocusing has been proposed based on the "shifted-beam theory" [7], where conventional antenna-array theory has been reformulated for near-field analysis. This concept utilizes the radiation emanating from spatially displaced antennas, also referred to as the "shifted beams," to facilitate the evanescent wave interference phenomenon. An arbitrary near-field waveform can be easily synthesized by weighting and summing these beam patterns, although practical limitations associated with the implementation of these structures usually restrict the achievable waveforms, which, in turn, limit the resolution. These limitations include the interelement spacing between the antennas and the required precision on the amplitude and phase of their radiated fields. Nevertheless, using this approach, antenna arrays with subwavelength separation (0.15λ) between the elements have been demonstrated capable of achieving subdiffraction imaging at a working distance as large as a quarter-wavelength [7]. What is remarkable about this approach is that it is not sensitive to material losses, which have severely limited the performance of metamaterial superlenses previously. Although this work has been carried out in the microwave domain, adaptations of the shifted-beam

technique, namely, "metascreens" consisting of 1D slot antenna arrays, have been shown to provide similar advantages for optical applications [8]. Another proposed related technique makes use of the high-order modes of plasmonic waveguides to achieve 1D optical focusing farther away from the imaging elements [9]. However, more practical configurations that can achieve two-dimensional (2D) focusing at optical frequencies are still lacking.

It is the purpose of this paper to combine the techniques used in microwave shifted-beam antenna-arrays with those available for the domain of optical instruments and fabrication in order to achieve 2D subdiffraction focusing beyond the extreme near field. To this end, recent work on fabricating a plasmonic monopole at the facet of a SNOM aperture probe has been demonstrated at 514 nm using focused-ion-beam (FIB) lithography [10]. It is hereby recognized that this work presents a practical platform for implementing monopole antenna-array type of structures in the visible wavelength regime. In this paper, we propose a design that incorporates a "ring" of satellite monopole antennas arranged in a rotationally symmetric configuration around the central monopole, as illustrated in Fig. 1. The apertures are also incorporated to excite the monopoles effectively, as discussed in Section 2. This 2D planar array is inspired by its microwave counterpart [11,12], and is hereby shown to reduce the diffraction-limited focal spot size of a single monopole radiation by 40% at a working distance of $\lambda/4$. More importantly, the satellite elements are able to significantly diminish the background noise signal (see Section 4), which enables subdiffraction imaging with a higher signal-to-noise ratio.

2. BACKGROUND

At optical frequencies, the transmission through the probe aperture can be utilized to effectively excite the monopole antenna in a way that is similar to its microwave counterpart being excited by a coaxial cable [10,13]. Although similar to microwave antennas in principle, the optical implementation exhibits its own special features. First, its physical length is much shorter than the conventional $\lambda/4$. This peculiar scaling effect, observed in plasmonic antennas in general, has been theoretically and numerically analyzed [14,15]. Furthermore, due to practical limitations of nanofabrication, such as those imposed by FIB lithography, the resulting antenna radius is very large at visible frequencies (approximately $1/25\lambda$ at 514 nm) compared to its microwave counterpart, which is usually less than a few hundredths of λ. As a result, the closed-form solution of an ideal perfect-conducting monopole with infinitesimally thin arms cannot accurately represent its end-fire radiation [16]. Numerical analysis tools, in particular, the commercial software package COMSOL Multiphysics, based on the finite element method, has been employed for accurately predicting the monopole radiation. Moreover, we would like to point out several works regarding optical coaxiallike waveguides [17,18], some of which also find applications in near-field imaging and spectroscopy [19]. However, these coax waveguides are not suitable for exciting the monopole antenna. This is because, unlike microwave coaxial cables that support the fundamental TEM mode, the optical coaxiallike waveguides produce only modes of "odd" azimuthal order when excited by a linearly polarized plane wave due to the symmetric electric field distribution with respect to the center pin [18,19]. As a result, they produce a null for the E_z component at the center pin, which means that the monopole at this location cannot be excited. Finally, the aperture illumination leads to nonuniform excitation of the monopole, depending on the angle between the monopole and the polarization of illumination. For example, as the one illustrated in Fig. 2, where the illumination in the optical probe is polarized in the x direction, the monopole is excited with maximum amplitude when it is aligned with the x axis. Furthermore, placing monopoles on opposite edges of the aperture leads to radiation with opposite phases. This, along with changing the aperture size and the monopole length, provides an effective way of engineering both the magnitude and the phase of the monopole end-fire radiation in the near field.

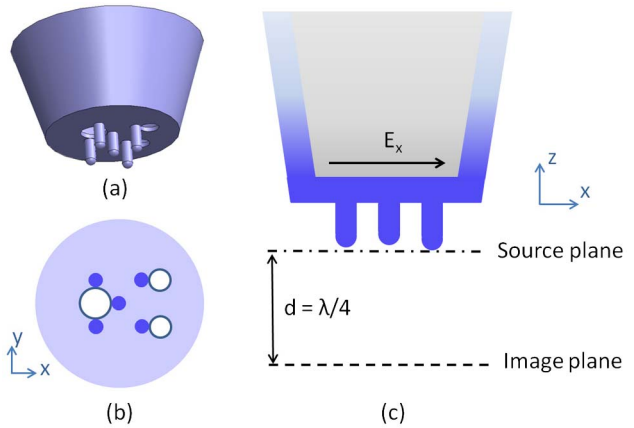

Fig. 1. (Color online) Proposed topology of a 2D near-field monopole array at the end facet of a SNOM aperture probe. The design is intended to operate at 514 nm, and the monopoles are made of aluminum with $\epsilon_r = -31.3 - j8$. The antenna array consists of one central and four satellite elements, with a center-to-satellite interelement spacing of 100 nm (about 0.193λ). The left illuminating aperture has a diameter of 100 nm and the right ones are 70 nm. The lengths of the left, central, and right monopoles are 80, 75, and 85 nm, respectively, and the radii are 20 nm. (a) Optical probe configuration, (b) the rotationally symmetric arrangement of the antenna array at the end facet (transverse plane), and (c) the respective locations of the source and image planes along the longitudinal direction.

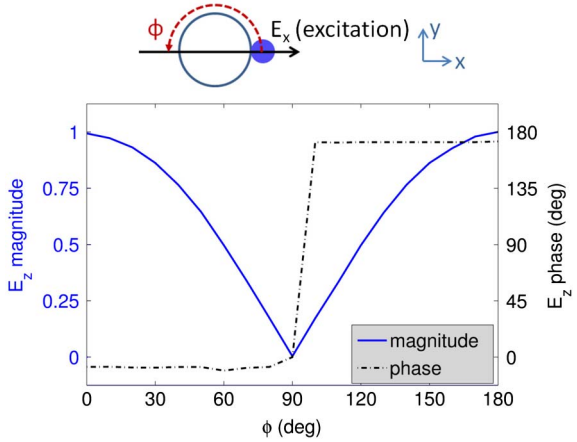

Fig. 2. (Color online) End-fire radiation of the monopole antenna when the aperture is illuminated with a plane wave polarized in the x direction. The monopole antenna is placed along the aperture edge at various angles with respect to the direction of illumination. The electric field is obtained at 1 nm below the apex of the antenna.

Imaging with such an optical monopole exhibits several advantages compared to using the aperture alone. Because of its small geometry, the near-field resolution at the antenna apex is much higher compared to the aperture, which is typically 50–100 nm in diameter. Additionally, the monopole radiates strongly at resonance, which facilitates efficient energy coupling from the, otherwise optically small, aperture to free-space radiation. (The near-field radiation intensity is further discussed in Section 4.)

However, using this structure to illuminate beyond the extreme near field is problematic because the fields introduced by the aperture interfere with the end-fire monopole radiation, thus producing an unwanted sidelobe, as shown in Fig. 3(a). This sidelobe, which effectively acts as background noise, becomes comparable in strength to the main beam with increased imaging distance, hence severely reducing the resolving power. As illustrated in Fig. 3(b), the beam width at a quarter-wavelength away has a full width at half-maximum (FWHM) of 0.48λ along the y axis, which represents Abbe's diffraction limit, whereas the one along the x axis is blurred by the background noise. Note that we select the image location at $z = \lambda/4$ as our benchmark for achieving the subdiffraction focusing because the FWHM coincides with the conventional diffraction limit. In this work, the FWHM is defined with respect to the magnitude of the electric field (instead of the intensity) in order to maintain consistency with previous relevant work in the microwave regime [11,12]. The results for the electric field intensity are presented in Fig. 6 for completeness.

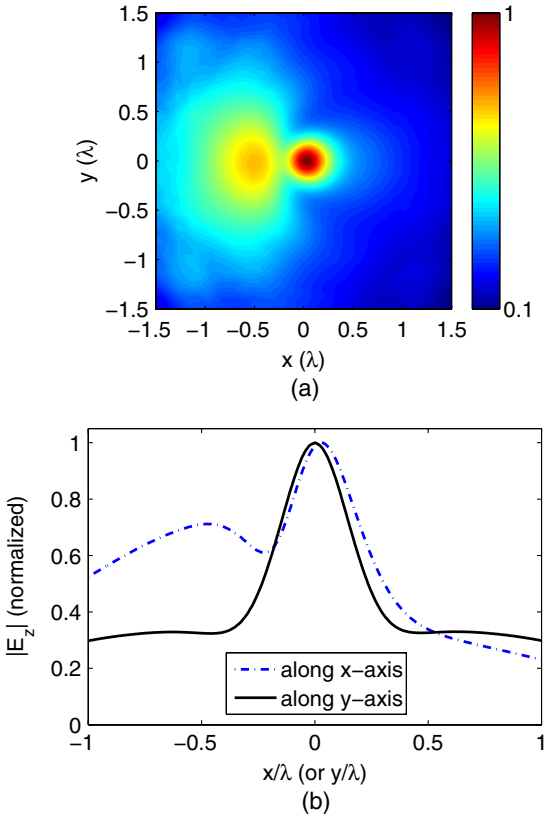

Fig. 3. (Color online) $|E_z|$ at the image plane ($z = 0.25\lambda$) for the single monopole configuration. The monopole antenna is excited with a probe aperture of 100 nm in diameter, and the incident electric field is polarized along the x direction. (a) $|E_z|$ in the transverse plane and (b) $|E_z|$ in the transverse plane along the x and y axes. In this case, the beam width along the x axis is blurred by the noise introduced by the probe aperture, while the one along the y axis represents the diffraction limit.

3. DESIGN METHODOLOGY

The purpose of our design is to obtain a subdiffraction focal spot at the image plane. We achieve this by constructing spatially shifted beams" which, in a 2D configuration, translates to positioning a ring of satellites around the central radiator. The essential design criterion is to obtain opposite phases between the central monopole and its satellites, such that their end-fire radiation in the near field can interfere destructively to sharpen the diffraction-limited single-beam radiation [7,12]. The relative magnitude of the satellite radiation, along with the separation distance, determines the amount of beam width reduction. In general, a small separation distance allows for achieving a small focal spot size. Given a fixed separation, a stronger satellite radiation can further reduce the main beam width, but at the expense of an increased sidelobe level.

At microwave frequencies, this is achieved by directly exciting the central monopole with a coaxial cable, and the satellite elements are excited indirectly through mutual coupling. The out-of-phase radiation is due to the mutual impedance between resonant monopoles separated with subwavelength distances [16]. For the specific design presented in [11,12], the amplitude of the satellite radiation can reach 1/2 of that of the main beam for a central-to-satellite separation of 0.15λ. The corresponding focal spot size at a quarter-wavelength imaging distance is shown to be 60% less than the diffraction limit.

In the visible regime, the large aperture used for exciting the central monopole antenna disrupts the planar symmetry. Besides introducing asymmetrically distributed background noises, this excitation scheme does not allow satellite monopoles to be placed at the nominal distance of 0.15λ (77 nm) from all directions [see Fig. 1(b)]. Therefore, the separation distance has to be increased to about 0.193λ (100 nm) to allow for placing four satellite monopoles with a planar rotational symmetry. The increased separation distance will increase the achievable optical spot size. On the other hand, the satellite radiation due to mutual coupling is only 1/5 of the main beam at 514 nm. Therefore, excitation for the satellites through other means is necessary to enhance their radiation. To this end, we introduce additional apertures to directly excite the satellite elements instead of relying on mutual coupling alone. The amplitude and phase of the excitation can be controlled through changing the position of the monopoles along the aperture edge with respect to the polarization of the incident waves, as well as adjusting the aperture size and the monopole length, as discussed in Section 2. In our design, we try to minimize the number of additional apertures in order to reduce the overall background noise. Therefore, only the two satellite monopoles on the right are excited with smaller apertures, whereas the left ones are placed directly on the edge of the aperture that also excites the central monopole.

In our design, the left, central, and right monopoles are all made of aluminum, and have lengths of 80, 75, and 85 nm, respectively, which correspond to antenna lengths that are slightly longer than the resonance at $\lambda = 514$ nm. We design the central radiator to operate closest to the resonance to

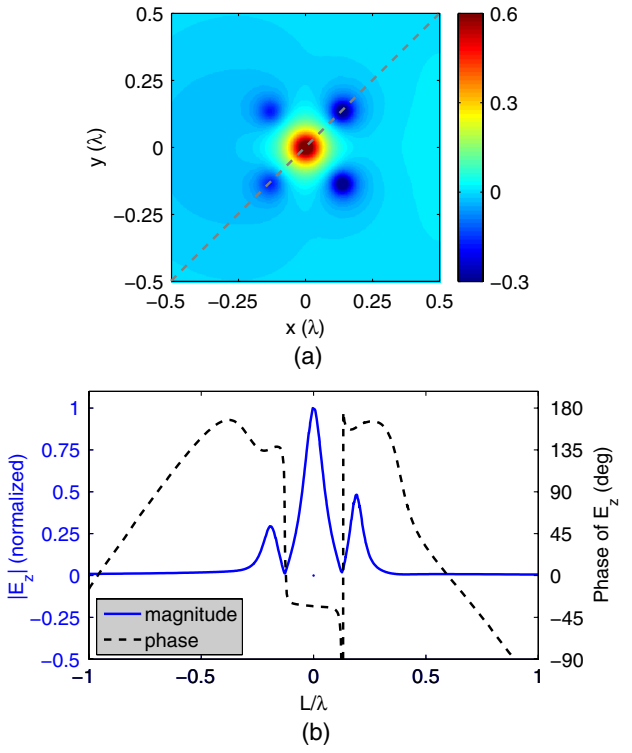

Fig. 4. (Color online) Field distribution (E_z) at the source plane ($z = 0$). (a) The planar distribution shows that the central and the satellite monopoles are radiating with opposite phases. (b) Comparison of the magnitude and the phase among the left, central, and right elements along the dashed line in (a). The normalized weights and the relative phases are (0.3, 1, 0.5) and (179°, 0°, −165°), respectively.

ensure the maximum radiation. The satellite monopole lengths are then adjusted to control the amount of interference. The left aperture is 100 nm in diameter, whereas the smaller ones on the right are 70 nm, which facilitates a weaker excitation for the satellites compared to the central radiator. These antenna lengths and aperture sizes can be physically implemented using FIB technology [10]. The resulting source distribution is illustrated in Fig. 4, where the normalized amplitudes of the left and the right satellites are 0.3 and 0.5, with corresponding phases of 179° and −165° with respect to the central monopole.

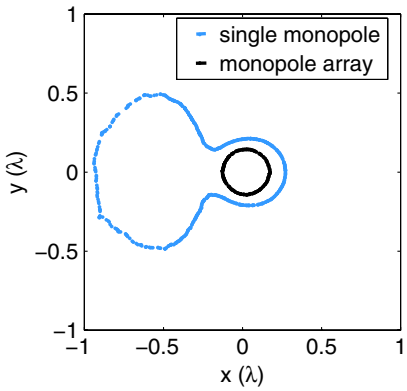

Fig. 5. (Color online) Contour diagram of the FWHM of $|E_z|$ at the image plane ($z = 0.25\lambda$). A comparison is made between the beam width of the single monopole (blue/light) and the monopole array (black/dark).

4. RESULTS AND DISCUSSION

The improvement of the monopole array over the single monopole when imaging at a $\lambda/4$ distance can be illustrated through two performance measures, namely, the reduced FWHM of the focal spot size and the diminished aperture noise interference. With respect to the reduced FWHM, the contour diagram of the magnitude $|E_z|$ at the image plane is shown in Fig. 5. Compared to the diffraction-limited beam width of the single monopole (blue/light), the smaller focal

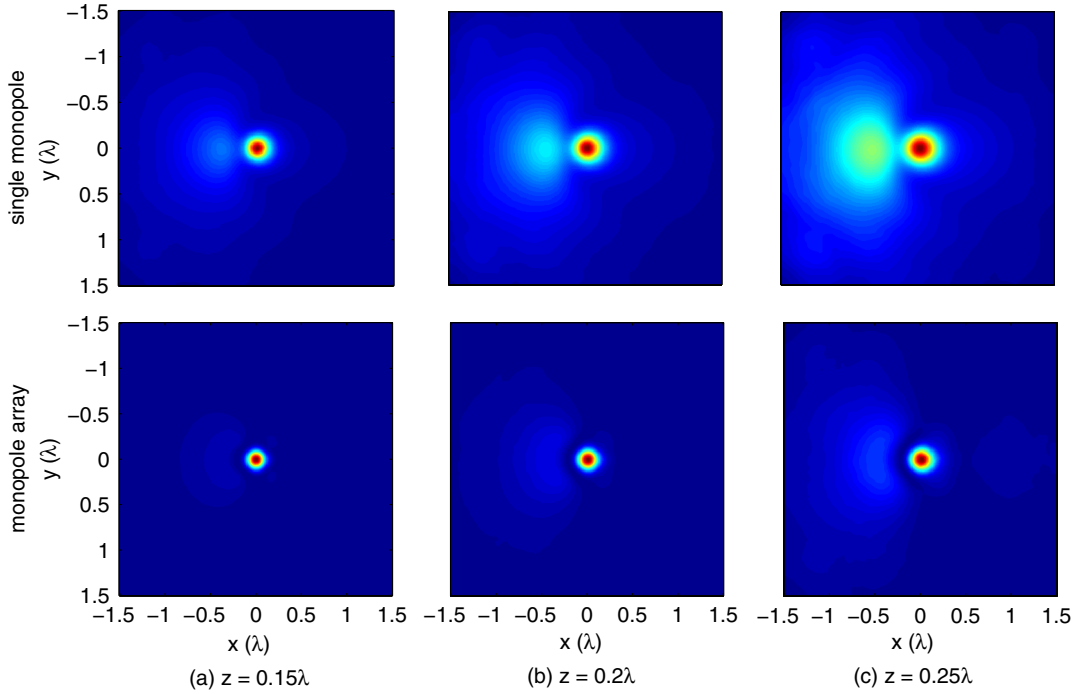

Fig. 6. (Color online) Comparison of the normalized field intensity ($|E_z|^2$) of the single monopole and the monopole array at various imaging distances.

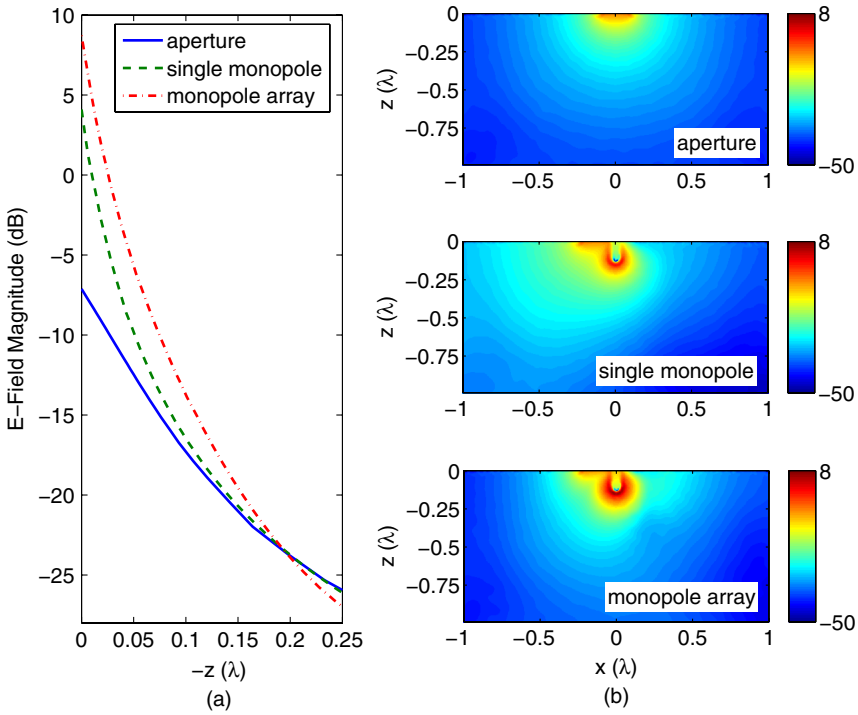

Fig. 7. (Color online) Magnitude of electric field in the near field of the single aperture, single monopole, and monopole array. ($|E_{\text{excitation}}| = 0$ dB for all three cases). (a) E-field magnitude versus the working distance. In the case of the single aperture probe, the working distance is measured from the center of the aperture. For the single monopole and the monopole array excited by aperture(s), the working distance is measured from the apex of the (central) monopole. (b) Magnitude (in decibels) of the E-field distribution in the x–z plane.

spot from the monopole array (black/dark) indicates that the beam width is subdiffractional. More specifically, the FWHM of the array beam width is 0.29λ along the y axis, which represents about 40% reduction from the diffraction limit. On the other hand, the resolving power along the x axis increases tremendously due to the reduction of the interference from the aperture noise. Note that the source configuration that produces the smallest focal spot size does not provide the strongest suppression of the background noise. For our design, a compromise has been made for achieving a symmetric 2D FWHM distribution with a 40% spot size reduction, while maintaining the noise intensity of 17% of the main beam. We would like to emphasize that the benefit of noise reduction becomes increasingly important at longer imaging distances, as shown in Fig. 6. We can see that the intensity of the aperture noise becomes more comparable to the main beam when the imaging distance increases from 0.15λ to 0.25λ. Therefore, the advantage of utilizing antenna arrays becomes more apparent when operating at long distances.

Another advantage of such a topology is that it increases the near-field intensity of the optical probe compared to the traditional aperture probe. As illustrated in Fig. 7, the magnitude of the electric field is analyzed for the aperture, the single monopole, and the monopole array when the excitation electric field has a magnitude of 0 dB for all three cases. It indicates that the plasmon resonance of the monopole antenna enhances the electric field around its apex, which produces a higher field intensity compared to the illuminating aperture alone. Note that the field amplification is more beneficial when imaging in closer proximity of the antenna apex due to the fast divergence of evanescent fields. As illustrated in Fig. 7(a), the electric field strength from the monopole end-fire radiation is stronger than the one transmitted through the aperture probe within a working distance of 0.2λ. The field strengths are still comparable at a working distance of 0.25λ. This demonstrates the potential of the monopole array structure as a practical solution for near-field measurements, where the working distance and the insertion loss can be extended beyond what is currently available for the SNOM instruments.

5. CONCLUSION

In conclusion, we present a planar plasmonic antenna array that achieves 2D superfocusing at a large working distance at visible frequencies. The design applies antenna-array theories, such as the mutual coupling between resonant monopoles and the shifted-beam theory, for optical near-field applications. We demonstrate a 40% improvement over the diffraction-limited spot size at a working distance of $\lambda/4$ with strongly diminished background noise. The benefits of such a design for near-field applications can be illustrated as follows: first, the monopole antenna array radiates strongly at resonance, producing a high signal-to-noise ratio. Second, the proposed configuration enables subdiffraction focusing at a much longer distance than what has been demonstrated in previous attempts. This is beneficial for high-resolution optical imaging because a longer working distance reduces the near-field disturbance during measurements due to the invasive presence of the probes. Moreover, although the proposed configuration is designed for the visible regime, this topology is scalable to other spectra as well. Finally, this design is compatible with existing near-field microscopy techniques and can, thus, be potentially incorporated in commercial scanning near-field optical microscopes.

REFERENCES

1. A. Grbic and G. V. Eleftheriades, "Overcoming the diffraction limit with a planar left-handed transmission-line lens," Phys. Rev. Lett. **92**, 117403 (2004).
2. N. Fang, H. Lee, C. Sun, and X. Zhang, "Sub-diffraction-limited optical imaging with a silver superlens," Science **308**, 534–537 (2005).
3. A. K. Iyer and G. V. Eleftheriades, "Mechanisms of subdiffraction free-space imaging using a transmission-line metamaterial superlens: an experimental verification," Appl. Phys. Lett. **92**, 131105 (2008).
4. E. Betzig and J. K. Trautman, "Near-field optics: microscopy, spectroscopy, and surface modification beyond the diffraction limit," Science **257**, 189–195 (1992).
5. R. Merlin, "Radiationless electromagnetic interference: evanescent-field lenses and perfect focusing," Science **317**, 927–929 (2007).
6. A. Grbic, L. Jiang, and R. Merlin, "Near-field plates: subdiffraction focusing with patterned surfaces," Science **320**, 511–513 (2008).
7. L. Markley, A. M. H. Wong, Y. Wang, and G. V. Eleftheriades, "A spatially shifted beam approach to subwavelength focusing," Phys. Rev. Lett. **101**, 113901 (2008).
8. Y. Wang, A. M. H. Wong, L. Markley, A. S. Helmy, and G. V. Eleftheriades, "Plasmonic meta-screen for alleviating the trade-offs in the near-field optics," Opt. Express **17**, 12351–12361 (2009).
9. R. Gordon, "Proposal for superfocusing at visible wavelengths using radiationless interference of a plasmonic array," Phys. Rev. Lett. **102**, 207402 (2009).
10. T. H. Taminiau, F. B. Segerink, and N. F. van Hulst, "A monopole antenna at optical frequencies: single-molecule near-field measurements," IEEE Trans. Antennas Propag. **55**, 3010–3017 (2007).
11. L. Markley and G. V. Eleftheriades, "Two-dimensional subwavelength-focused imaging using a near-field end-fire antenna-array probe," IEEE Antennas Wirel. Propag. Lett. **8**, 1025–1028 (2009).
12. L. Markley and G. V. Eleftheriades, "Two-dimensional subwavelength-focused imaging using a near-field probe at a $\lambda/4$ working distance," J. Appl. Phys. **107**, 093102 (2010).
13. T. H Taminiau, F. B. Segerink, R. J. Moerland, L. Kuipers, and N. F. van Hulst, "Near-field driving of a optical monopole antenna," J. Opt. Pure Appl. Opt. **9** S315–S321 (2007).
14. L. Novotny, "Effective wavelength scaling for optical antennas," Phys. Rev. Lett. **98**, 266802 (2007).
15. G. W. Bryant, F. J. García de Abajo, and J. Aizpurua, "Mapping the plasmon resonances of metallic nanoantennas," Nano Lett. **8**, 631–636 (2008).
16. C. A. Balanis, *Antenna Theory: Analysis and Design*, 2nd ed. (Wiley, 2004).
17. F. I. Baida, A. Belkhir, D. Van Labeke, and O. Lamrous, "Subwavelength metallic coaxial waveguides in the optical range: role of the plasmonic modes," Phys. Rev. B **74**, 205419 (2006).
18. R. de Waele, S. P. Burgos, A. Polman, and H. A. Atwater, "Plasmon dispersion in coaxial waveguides from single-cavity optical transmission measurements," Nano Lett. **9**, 2832–2837 (2009).
19. A. Weber-Bargioni, A. Schwartzberg, M. Cornaglia, A. Ismach, J. J. Urban, Y. Pang, R. Gordon, J. Bokor, M. B. Salmeron, D. F. Ogletree, P. Ashby, S. Cabrini, and P. J. Schuck, "Hyperspectral nanoscale imaging on dielectric substrates with coaxial optical antenna scan probes," Nano Lett. **11**, 1201–1207 (2011).